

An Asynchronous Mixed-Signal Resonate-and-Fire Neuron

Giuseppe Leo*, Paolo Gibertini*, Irem Ilter†, Erika Covi*, Ole Richter‡§, Elisabetta Chicca*

*Zernike Institute for Advanced Materials and Groningen Cognitive Systems and Materials Centre (CogniGron),
University of Groningen, Groningen, The Netherlands

†Electrical and Electronics Engineering, Bilkent University, Ankara, Turkey

‡Asynchronous Integrated Circuits, Embedded Systems Engineering, DTU Compute, Technical University of Denmark, Denmark

§Asynchronous VLSI and Architecture Group, School of Engineering and Applied Science, Yale University, CT, USA

Email: {g.leo, p.gibertini, e.covi, e.chicca}@rug.nl, irem.ilter@ug.bilkent.edu.tr, ojuri@dtu.dk

Abstract—Analog computing at the edge is an emerging strategy to limit data storage and transmission requirements, as well as energy consumption, and its practical implementation is in its initial stages of development. Translating properties of biological neurons into hardware offers a pathway towards low-power, real-time edge processing. Specifically, resonator neurons offer selectivity to specific frequencies as a potential solution for temporal signal processing. Here, we show a fabricated Complementary Metal-Oxide-Semiconductor (CMOS) mixed-signal Resonate-and-Fire (R&F) neuron circuit implementation that emulates the behavior of these neural cells responsible for controlling oscillations within the central nervous system. We integrate the design with asynchronous handshake capabilities, perform comprehensive variability analyses, and characterize its frequency detection functionality. Our results demonstrate the feasibility of large-scale integration within neuromorphic systems, thereby advancing the exploitation of bio-inspired circuits for efficient edge temporal signal processing.

I. INTRODUCTION

Neurons differ in form and function, and this diversity enables the brain to produce its rich repertoire of capabilities [1]. Spiking neurons can be classified according to their electrophysiological behaviour [2]. Leaky Integrate-and-Fire (LIF) neurons [3], predominant in modern Spiking Neural Network (SNN) architectures, act as integrators, responding mainly to the average amplitude of the input; they belong to Class I, which is characterized by a continuous frequency–current (F-I) curve. Resonator neurons [4], whose response depends primarily on spike timing, are part of Class II; they exhibit a discontinuous F-I curve, initiating high-frequency firing above a specific threshold. They drive oscillatory activity, that controls functional states and coordinates muscular activity within the central nervous system [5, 6].

The Resonate-and-Fire (R&F) neuron model [7], along with its variants [8–11], captures these biological behaviours compactly. It can exhibit rhythmic firing under constant stimulation and resonance to sparse inhibitory and excitatory inputs, showing selectivity to specific frequencies, a property that can be exploited in sensory processing and temporal pattern recognition applications. It has been successfully tested mainly in simulation across a range of applications, including

associative memories [12], optical flow estimation [13], radar signal processing [14–16], voice detection [17], and gesture recognition [18]. However, simulations are too computationally expensive for efficient real-time applications. To address this, digital Application-Specific Integrated Circuit (ASIC) implementations have been proposed [13, 19, 20]. They typically rely on time-stepped numerical integration of differential equations and extensive memory updates. In contrast, analog circuits are able to exploit the inherent parallelism and continuous-time operation of the physical model. To date, only a few analog implementations of R&F neurons have been proposed and simulated [21] or fabricated [22, 23].

In this work, we present and characterize an enhanced Complementary Metal-Oxide-Semiconductor (CMOS) implementation of the R&F neuron (Fig. 1) originally proposed by Nakada *et al.* [21]. Our design features sub-threshold analog membrane potential dynamics and digital output spikes integrated with asynchronous handshaking for compatibility with neuromorphic hardware platforms based on Address-Event Representation (AER) communication [24]. We fully characterized the circuit in silico across one hundred dies. Specifically, we measured variability in system parameters and overall power consumption. Furthermore, we demonstrated the selectivity properties of the spiking response with respect to the frequency of the input spike train. We supplemented the experimental results with a broad yet low-resolution analysis of the circuit’s operational range and energy consumption per spike using post-layout simulation. These results suggest suitability for real-time, low-power processing of audio, elec-

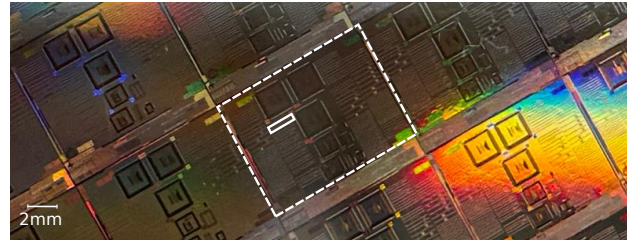


Fig. 1: Photograph of the fabricated wafer containing multiple dies. The dashed white rectangle highlights one die and the solid lined rectangle delimits the test structure that includes the R&F neuron, the I/O circuits, and the pads ($122\mu\text{m} \times 1772\mu\text{m}$). The neuron has an area of $35\mu\text{m} \times 155\mu\text{m}$.

This work was supported by the European Research Council (ERC) through the European Union’s Horizon Europe Research and Innovation Programme under Grant Agreements No. 101119062 and 101042585. The authors would like to acknowledge the financial support of the CogniGron research center and the Ubbo Emmius Funds (Univ. of Groningen).

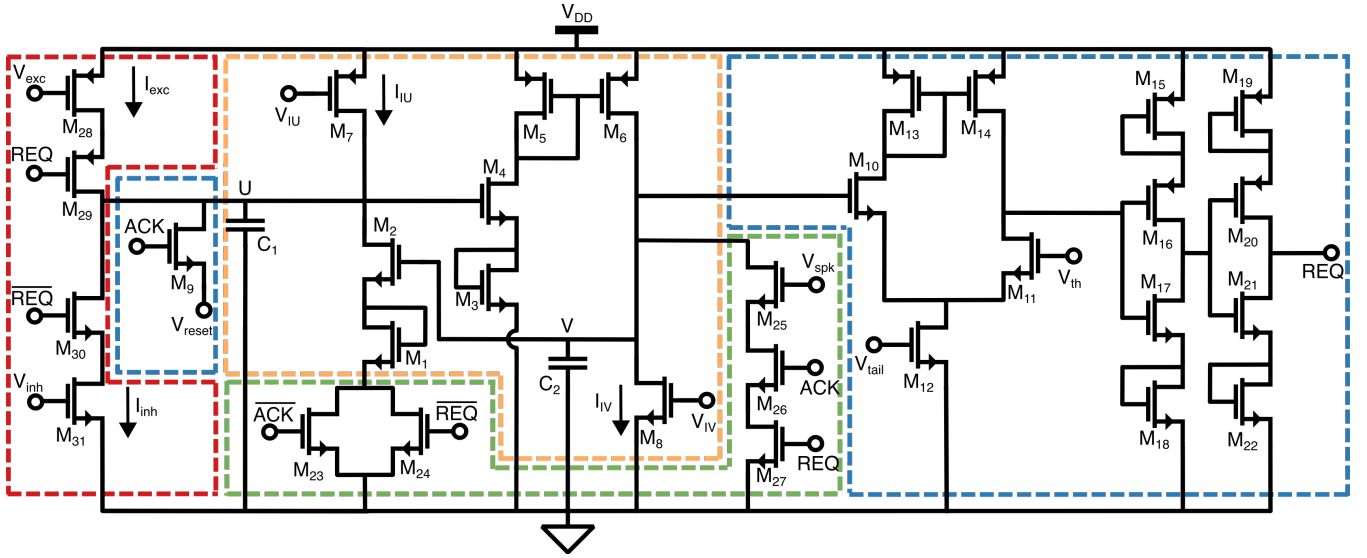


Fig. 2: Schematic of the R&F circuit. The four functional blocks are highlighted in the circuit: in red, the two analog synapses, in orange, the resonator, in green, the handshake logic, and in blue, the spike generator.

tromyography (EMG) and electrocardiography (ECG) signals.

II. CIRCUIT DESCRIPTION

The circuit architecture (Fig. 2) consists of four main functional blocks: a resonator, a spike generator, a handshake logic, and two analog synapses (one inhibitory and one excitatory).

1) *Resonator Circuit* ($M_1 - M_8$): The circuit's core oscillatory dynamics are based on [21] and are realized through a modified Lotka-Volterra (LV) oscillator [25]. A dynamical system with a stable focus equilibrium can be obtained by precisely tuning the circuit's loop gain and the currents I_{IV} and I_{IU} (through voltages V_{IV} and V_{IU}). Taking into account the exponential dependence of the current on the gate voltage for sub-threshold circuits, the circuit dynamics can be modeled by

$$C_1 \frac{dU}{dt} = I_{in} + I_{IU} - I_{n0} \exp\left(\frac{\kappa_n^2}{\kappa_n + 1} \frac{V}{U_T}\right) \quad (1)$$

$$C_2 \frac{dV}{dt} = I_{n0} \exp\left(\frac{\kappa_n^2}{\kappa_n + 1} \frac{U}{U_T}\right) - I_{IV} \quad (2)$$

where U and V are the voltages across capacitors C_1 and C_2 respectively, I_{n0} depends on the transistors' fabrication process and geometry, U_T is the thermal voltage and κ_n is the transistors' capacitive coupling coefficient. I_{in} is the summation of the synaptic currents, I_{exc} and I_{inh} . The currents I_{IU} and I_{IV} are parameters that control the neuron's resonant frequency. Under the change of variable $I_\alpha = I_{n0} \exp[U\kappa_n^2/((\kappa_n + 1)U_T)]$ (and equivalent I_β for V), (1) and (2) become

$$\frac{dI_\alpha}{dt} \propto I_\alpha (I_{in} + I_{IU} - I_\beta) \quad (3)$$

$$\frac{dI_\beta}{dt} \propto I_\beta (I_\alpha - I_{IV}) \quad (4)$$

which are the LV equations for a 2-variable predator-prey system [25]. When expanded around the system's equilibrium point [21], (3) and (4) approximate the R&F dynamics [7], expressed by

$$\frac{du}{dt} = bu - \omega v + cI \quad (5)$$

$$\frac{dv}{dt} = \omega u + bv \quad (6)$$

where u and v represent the system state variables, $b < 0$ is the decay factor, ω is the resonant frequency of the system, I represents the total external input, and c is the synaptic weight.

2) *Spiking Circuit* ($M_9 - M_{22}$): In order to detect when the voltage V becomes higher than the threshold V_{th} and trigger a request (REQ) signal, a simple comparator is used ($M_{10} - M_{14}$). The output is routed through a cascade of two inverters ($M_{15} - M_{22}$), which are designed to limit the current through diode connected transistors. The sharp output of the inverter chain is used as REQ in the handshake protocol. While the REQ signal is high, the variable U is reset to V_{reset} through transistor M_9 .

3) *Handshake logic* ($M_{23} - M_{27}$): To enable event-based communication, the circuit integrates an asynchronous handshake mechanism [26]. After the REQ signal becomes high and for the duration of the handshake, the membrane potentials U and V are held stable to prevent spurious dynamics. U is stabilized at V_{reset} and V at V_{th} by means of the transistors $M_{23} - M_{24}$ and $M_{25} - M_{27}$, respectively. Once an acknowledge (ACK) signal is received, the normal dynamics resume, allowing the neuron to re-enter its oscillatory regime. The bias V_{spk} modulates the duration of the spike.

4) *Synapses* ($M_{28} - M_{31}$): The synapses (excitatory, $M_{28} - M_{29}$, and inhibitory, $M_{30} - M_{31}$) are implemented as direct transistor-based voltage-controlled current generators and allow the neuron to process both spiking inputs and continuous

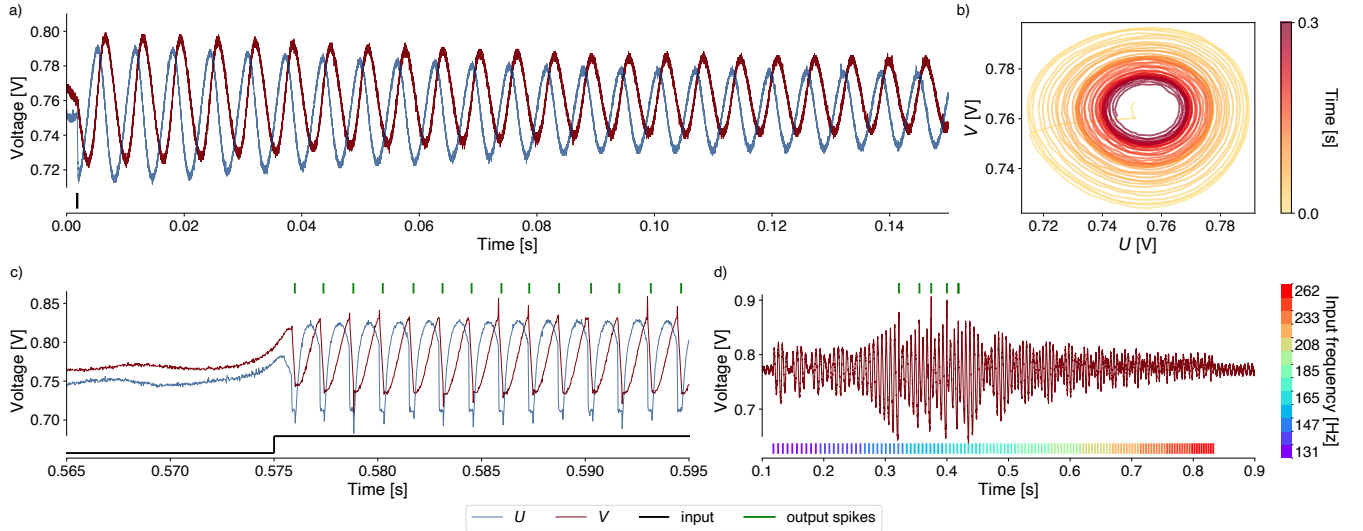


Fig. 3: Measured membrane voltage dynamics for spikes and constant input. (a) Time-domain (up to 0.15 s) and (b) phase-plane dynamics (up to 0.3 s) after one inhibitory input. (c) Rhythmic firing in response to step excitatory stimulation, with a baseline value of 0 V and a step value of 0.5 V. (d) Response to an up-chirp consisting of 10 spikes per frequency across a total of 13 frequencies. It shows frequency-selective spiking around 150 Hz. The spike input in a) and d) has a time width of 100 μ s and an amplitude of 0.5 V. We define the inhibitory input voltage as V_{inh} and the excitatory input voltage as $V_{\text{DD}} - V_{\text{exc}}$.

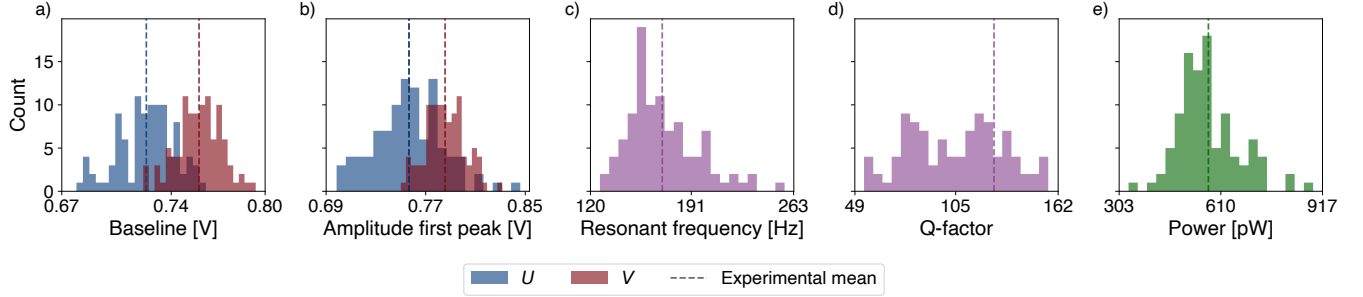


Fig. 4: Measured die-to-die variability (100 dies). (a) Baseline voltage distributions for U (mean value 724 mV) and V (mean value 758 mV). (b) First peak amplitude distributions for U (mean value 757 mV) and V (mean value 786 mV). (c) Resonant frequency distributions (mean value 170 Hz). (d) Q-factor distributions (mean value 129). (e) Distribution of the power consumption (mean value 571 pW).

signals. Transistors M_{29} and M_{30} prevent synaptic current to flow through the circuit during the handshake.

III. RESULTS

The circuit was fabricated in 180-nm CMOS technology for cost-effective prototyping, along with multiple other test structures on the *chip-Olla* ASIC and resulted in an area of $35 \mu\text{m} \times 155 \mu\text{m}$, mainly due to the size of the capacitors ($C_1, C_2 = 1.2 \text{ pF}$).

The two analog membrane-potential signals and the digital spike output are routed off-chip through separate buffer stages. For all characterization experiments, the REQ signal was externally connected to the ACK line for self-acknowledge [26]. The experimental characterization of the circuit was carried

out with three experiments (Fig. 3). In the first, we measured the circuit dynamics following the application of an inhibitory pulse. In the second, we analyzed the neuron response to a constant input to validate Class II excitability. In the third, we measured the response to a spiking chirp signal, to study the neuron frequency selectivity property. The default operating parameters and biases used for the characterization are listed in Table I; in the second experiment, $V_{\text{th}} = 840 \text{ mV}$. The value of the bias current ($I_{\text{IU}} = I_{\text{IV}}$) is estimated by simulation and depends on the applied input bias voltages, V_{IV} and V_{IU} .

A. Internal dynamics analysis

The first measurement (Figs. 3a and 3b) investigates the response of the circuit to a negative input pulse, a key analysis to understand the generation of post-inhibitory spikes, i.e., firing following inhibitory stimulation. From these data, four system parameters were extracted — baseline voltage, first resonance peak amplitude, resonant frequency, and quality factor (Q-factor) — to assess fabrication-induced variability

TABLE I: Circuit bias parameters

V_{DD}	V_{th}	V_{reset}	V_{tail}	V_{spk}	$I_{\text{IU}}, I_{\text{IV}}$
1.5 V	850 mV	750 mV	300 mV	400 mV	150 pA

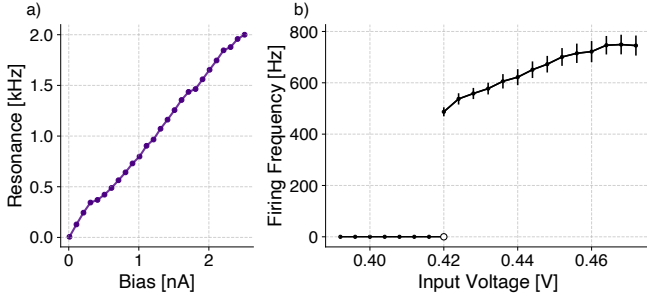


Fig. 5: (a) The resonant frequency depends linearly on the bias current (post-layout simulation results), ranging from 6 Hz at 10 pA to 2000 Hz at 2.51 nA. (b) F-I curve typical of Class II neurons (experimental results). The neuron is silent for inputs below 420 mV and exhibits high-frequency rhythmic firing for larger inputs. The empty circle in the graph represents this discontinuous behavior. Each point corresponds to the mean calculated from 100 spikes, with bars showing the standard deviation.

across multiple dies (Fig. 4). The low variability in the baseline (Coefficient of Variation (CV) = 2%) and in the amplitude of the initial oscillation (CV = 3%) is advantageous, as these parameters are critical for calibrating the spiking threshold bias. The resonant frequency and Q-factor define the system's resonance and decay characteristics, and their variability has a significant impact on frequency detection. The resonant frequency shows a CV of 15%, which is expected since it is related to variability in the threshold voltage of transistors M_2 and M_4 . The Q-factor exhibits substantial variability (CV = 68%), consistent with expectations due to its high sensitivity to process variations [21].

We measured power consumption variability to assess feasibility of deployment in large scale systems. We observed that the power consumption during the oscillation is approximately equal to the static power consumption; it has a mean value of 571 pW and a CV of 16%. Additionally, the estimate of the energy per spike over the entire spike duration through post-layout simulations was 196 fJ. These simulations (Fig. 5a) also indicate that the neuron's resonant frequency, estimated through a Fourier transform analysis, is tuneable between 6 Hz to 2000 Hz via parametrization of the circuit biases.

B. Neuronal transfer function

Experimental results (Fig. 3c) for one neuron confirm that it exhibits rhythmic firing under constant input. Fig. 5b shows the F-I relationship, highlighting the Class II discontinuity, after which the firing frequency scales with input.

Experimental measurements on the same die (Fig. 3d) evaluated the neuron's selectivity to specific input frequencies in the fine-grained range of 130 Hz to 260 Hz. As shown in Fig. 6, the circuit successfully detects specific frequencies depending on its biasing conditions. The implementation is highly flexible, as the range of detection can be adjusted via bias-current (I_{IU} and I_{IV}) tuning, while the resolution can be modified by adjusting the spiking threshold bias V_{th} .

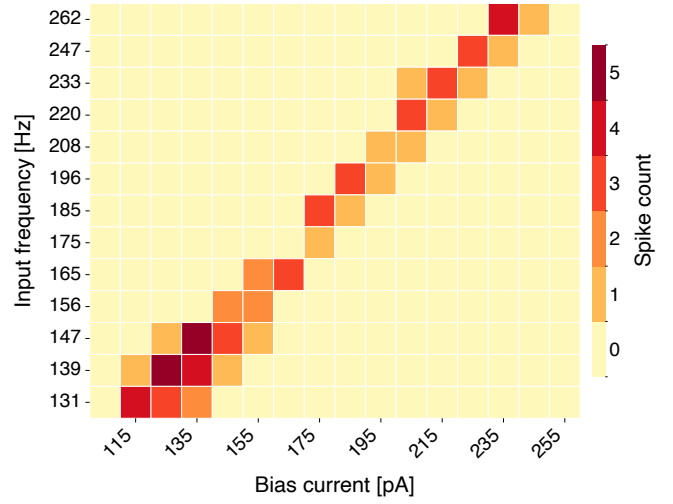


Fig. 6: Measured frequency detection. The input is a chirp signal from 131 Hz to 262 Hz. The bias currents ($I_{IU} = I_{IV}$) are varied from 105 pA to 255 pA to tune the neuron selectivity. The threshold voltage (V_{th}) increases exponentially with the bias from 840 mV to 900 mV. The results show that the neuron successfully detects specific frequencies according to the bias.

IV. CONCLUSION

The proposed R&F neuron implementation builds upon the circuit proposed in Nakada *et al.* [21]. Our additions include reduced power consumption, additional circuitry for embedding into AER transceiver chips [24], and extensive in-silico characterization comprising die-to-die variability.

Our design exhibits low power consumption (571 pW versus 2.34 μ W [21]) and low energy per spike (196 fJ, not reported in previous implementations). The study of the neuronal transfer function assessed the applicability of the system in sensory processing and band-pass filtering applications [27]. Since variability is a major challenge for the large-scale deployment of analog sub-threshold neuromorphic circuits, we performed extensive variability analyses. This proves that integration into broader neuromorphic systems [28, 29] is promising; we envision combining a bank of sub-threshold, asynchronous R&F neurons with bio-inspired analog spiking sensors [30, 31] to implement efficient, event-based edge-processing systems with greater expressivity than is achievable using Class I neurons only [32-34].

ACKNOWLEDGMENT

Thanks to Muath Abu Lebdeh, Hugh Greatorex, Madison Cotteret, Willian Soares Girão, and Giacomo Indiveri for their feedback. Ole Richter and Irem Ilter performed this work while at the University of Groningen.

REFERENCES

- [1] D. Purves *et al.*, *Neurosciences*. De Boeck Supérieur, Jul. 2025, google-Books-ID: 8xdxEQAAQBAJ.
- [2] J. Rinzel *et al.*, "Analysis of Neural Excitability and Oscillations," *MIT press Cambridge, MA*, vol. 2, 1998.
- [3] L. Abbott, "Lapicque's introduction of the integrate-and-fire model neuron (1907)," *Brain Research Bulletin*, vol. 50, no. 5-6, pp. 303-304, Nov. 1999.

- [4] B. Hutcheon *et al.*, "Resonance, oscillation and the intrinsic frequency preferences of neurons," *Trends in Neurosciences*, vol. 23, no. 5, pp. 216–222, May 2000, publisher: Elsevier.
- [5] R. R. Llinas, "The Intrinsic Electrophysiological Properties of Mammalian Neurons: Insights into Central Nervous System Function," *Science*, vol. 242, 1988.
- [6] X.-J. Wang, "Neurophysiological and Computational Principles of Cortical Rhythms in Cognition," *Physiological reviews*, 2010.
- [7] E. M. Izhikevich, "Resonate-and-fire neurons," *Neural Networks*, vol. 14, no. 6, pp. 883–894, Jul. 2001.
- [8] E. Izhikevich, "Simple model of spiking neurons," *IEEE Transactions on Neural Networks*, vol. 14, no. 6, pp. 1569–1572, Nov. 2003.
- [9] B. AlKhamissi *et al.*, "Deep Spiking Neural Networks with Resonate-and-Fire Neurons," Sep. 2021, arXiv:2109.08234 [cs].
- [10] S. Higuchi *et al.*, "Balanced Resonate-and-Fire Neurons," Oct. 2024, arXiv:2402.14603 [cs].
- [11] D. Zhang *et al.*, "Dendritic Resonate-and-Fire Neuron for Effective and Efficient Long Sequence Modeling," Sep. 2025, arXiv:2509.17186 [cs].
- [12] E. P. Frady *et al.*, "Robust computation with rhythmic spike patterns," *Proceedings of the National Academy of Sciences*, vol. 116, no. 36, pp. 18 050–18 059, Sep. 2019, publisher: Proceedings of the National Academy of Sciences.
- [13] G. Orchard *et al.*, "Efficient Neuromorphic Signal Processing with Loihi 2," Nov. 2021, arXiv:2111.03746.
- [14] S. Chiavazza *et al.*, "Low-Latency Spike-Based Range and Velocity Estimation of FMCW Radar Signals: 22nd European Radar Conference, EuRAD 2025," Sep. 2025.
- [15] N. Reeb *et al.*, "Range and angle estimation with spiking neural resonators for FMCW radar," *Neuromorphic Computing and Engineering*, vol. 5, May 2025.
- [16] J. Hille *et al.*, "Resonate-and-Fire Neurons for Radar Interference Detection," in *Proceedings of the International Conference on Neuromorphic Systems 2022*. Knoxville TN USA: ACM, Jul. 2022, pp. 1–4.
- [17] K. Shi *et al.*, "Spike-VAD: Efficient and Robust Spiking Neural Network for Voice Activity Detection," *IEEE Transactions on Cognitive and Developmental Systems*, pp. 1–13, 2025.
- [18] A. Shaaban *et al.*, "Resonate-and-Fire Spiking Neurons for Target Detection and Hand Gesture Recognition: A Hybrid Approach," May 2024, arXiv:2405.19351 [eess].
- [19] E. P. Frady *et al.*, "Efficient Neuromorphic Signal Processing with Resonator Neurons," *Journal of Signal Processing Systems*, vol. 94, no. 10, pp. 917–927, Oct. 2022.
- [20] T.-K. Le *et al.*, "Modeling and Designing of an All-Digital Resonate-and-Fire Neuron Circuit," *IEEE Access*, vol. 11, 2023.
- [21] K. Nakada *et al.*, "Analog VLSI implementation of resonate-and-fire neuron," *International journal of neural systems*, vol. 16, pp. 445–56, Jan. 2007.
- [22] K. Nakada *et al.*, "A subthreshold CMOS circuit for a piecewise linear neuromorphic oscillator with current-mode low-pass filters," *Neurocomputing*, vol. 71, no. 1, pp. 3–12, Dec. 2007.
- [23] H. M. Lehmann *et al.*, "Direct Signal Encoding With Analog Resonate-and-Fire Neurons," *IEEE Access*, vol. 11, pp. 50 052–50 063, 2023, conference Name: IEEE Access.
- [24] K. A. Boahen, "Point-to-point connectivity between neuromorphic chips using address events," *IEEE*, vol. 47, 2002.
- [25] N. S. Goel *et al.*, "On the Volterra and Other Nonlinear Models of Interacting Populations," *Reviews of Modern Physics*, 1971, publisher: American Physical Society.
- [26] J. Sparsø, *Introduction to asynchronous circuit design*. Kongens Lyngby, Denmark: DTU Compute, Technical University of Denmark, 2020, oCLC: 1199326564.
- [27] M. Mastella *et al.*, "Event-Driven Frequency Decomposition with Spiking Phase-Locked Loops," in *2024 58th Asilomar Conference on Signals, Systems, and Computers*, Oct. 2024, pp. 1517–1521, iSSN: 2576-2303.
- [28] H. Greatedorex *et al.*, "A neuromorphic processor with on-chip learning for beyond-CMOS device integration," *Nature Communications*, vol. 16, no. 1, p. 6424, Jul. 2025, publisher: Nature Publishing Group.
- [29] O. Richter *et al.*, "DYNAP-SE2: a scalable multi-core dynamic neuromorphic asynchronous spiking neural network processor," *Neuromorphic Computing and Engineering*, vol. 4, no. 1, p. 014003, Jan. 2024, publisher: IOP Publishing.
- [30] N. Bidoul *et al.*, "Bio-inspired Encoding of Heat Using VO2 Neuron Operated in Stochastic Bursting Regime," in *Proceedings of Neuronic Conference (Neuronic)*, 2023.
- [31] E. Janotte *et al.*, "Neuromorphic capacitive tactile sensors inspired by slowly adaptive mechanoreceptors," in *2022 20th IEEE Interregional NEWCAS Conference (NEWCAS)*. Quebec City, QC, Canada: IEEE, Jun. 2022, pp. 119–123.
- [32] M. Yao *et al.*, "Spike-based dynamic computing with asynchronous sensing-computing neuromorphic chip," *Nature Communications*, vol. 15, no. 1, p. 4464, May 2024.
- [33] S. Narayanan *et al.*, "SPAIC: A sub- μ W/Channel, 16-Channel General-Purpose Event-Based Analog Front-End with Dual-Mode Encoders," in *2023 IEEE Biomedical Circuits and Systems Conference (BioCAS)*. Toronto, ON, Canada: IEEE, Oct. 2023, pp. 1–5.
- [34] T. Schoepe *et al.*, "Closed-loop sound source localization in neuromorphic systems," *Neuromorphic Computing and Engineering*, vol. 3, no. 2, p. 024009, Jun. 2023, publisher: IOP Publishing.